

Viscous avalanches on a spherical minor planet

Deepayan Banik^{1,*} and Kumar Gaurav^{2,**}

¹Department of Physics, University of Toronto, Canada

²Indian Institute of Technology Kanpur, India

Abstract. Granular avalanches influence the surface evolution of small celestial bodies such as asteroids and moons. Understanding their dynamics is crucial for interpreting surface features observed by space missions. We adapt a depth-averaged shallow water model to simulate granular avalanches on a rotating, gravitating sphere, building on prior work by Gaurav et al. (2021) and Banik et al. (2022). Using the pseudo-spectral Dedalus code, we explore first-order granular motion by varying material friction and rotational speed. We simulate Gaussian hills of yielded material flowing under Coriolis forces. A limitation of our approach, like other spherical shallow water models, is inaccuracy near the poles, though results remain largely unaffected. Our findings provide benchmarks for future, more complex models incorporating spin change, thermal effects, and collisions.

1 Introduction

Granular avalanches or landslides play a pivotal role in shaping the surface morphology and evolution of small celestial bodies such as asteroids and moons. However, in most models, the effect of landslides on the spin evolution of rubble-pile asteroids is either neglected or been rarely considered. Recent studies have shown that spin-down due to surface regolith motion can be significant [1] to the extent of being comparable to the radiation driven spin-up over their near-Earth lifetimes [2]. These phenomena are not only central to understanding the current landscape of these bodies but also provide insights into their geological histories and the processes that govern their evolution.

Traditional approaches to modeling such flows have ranged from empirical models [3, 4] to more sophisticated continuum simulations. In particular, the work of [5] demonstrated the utility of continuum simulations for landslides on two-dimensional elliptical bodies, setting a foundation for more detailed investigations. Building on this, [2] extended these simulations to three-dimensional axisymmetric top-shapes, thereby capturing more realistic aspects of planetary surfaces. These studies collectively represent a framework to integrate avalanching in the overall evolution of rubble-pile asteroids.

We adapt a depth-averaged shallow water model to study localized granular avalanches on a rotating, gravitating sphere, potentially extending past axisymmetric assumptions. Using the pseudo-spectral code Dedalus [6], we examine first-order effects of friction and rotation. Certain assumptions constrain our model but enable analytical solutions verified by simulations. Despite its simplicity, our model yields generalized insights into global regolith

distribution from local landslides. We discuss limitations, including frictional approximations via viscosity and the polar singularity in spherical spectral methods. For a viscous fluid, regolith distribution remains axisymmetric, regardless of basal resistance or dune origin, supporting past axisymmetry assumptions over multiple landslides.

The remainder of the paper is organized as follows. In Section 2, we describe the mathematical formulation of our model and the numerical methods employed. Section 3 presents the simulation results, focusing on the dynamics of Gaussian hills of yielded material and the role of rotational forces. Finally, Section 4 discusses the implications of our findings and outlines directions for future work.

2 Mathematical model for dune motion

Consider a sphere rotating with angular velocity Ω . Let us call the gravitational acceleration at the surface \mathbf{g} . The components of the vector are given by,

$$\begin{aligned} \mathbf{g} \cdot \hat{r} &= g_n = g - \Omega^2 R \sin^2 \theta, \quad \mathbf{g} \cdot \hat{\phi} = 0, \\ \text{and } \mathbf{g} \cdot \hat{\theta} &= g_t = -\Omega^2 R \sin \theta \cos \theta \end{aligned} \quad (1)$$

We denote the normal and tangential components by g_n and g_t . The momentum and mass balances for a shallow water model with variables \mathbf{u} and h for velocity and height as applicable to the system are as follows,

$$\frac{\partial \mathbf{u}}{\partial t} + (\mathbf{u} \cdot \nabla) \mathbf{u} + 2\Omega \mathbf{k} \times \mathbf{u} + \nabla \cdot (g_n h) = -(\tan \delta) g_n \mathbf{u} + g_t \hat{\theta} \quad (2)$$

$$\frac{\partial h}{\partial t} + \nabla \cdot (h \mathbf{u}) = 0 \quad (3)$$

*e-mail: deepayan.banik@mail.utoronto.ca

**e-mail: kugaurav@iitk.ac.in

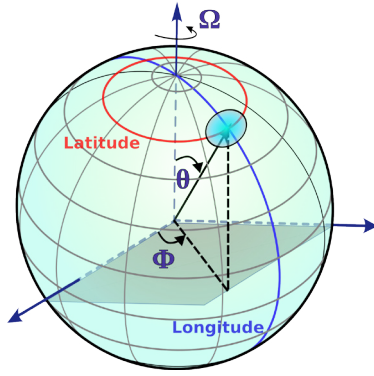


Figure 1. Schematic for the shallow water sphere setup showing co-latitude (θ , henceforth called latitude) and longitude (ϕ). The sphere rotates with angular velocity Ω and a small gaussian dune shown in blue serves as the initial condition.

where, \mathbf{k} is the unit vector along the axis of rotation. On the LHS, we have the unsteady, advective, Coriolis and pressure gradient terms. On the RHS, we have the resistive and body forces. Here, we approximate the surface material to be a highly viscous fluid, with the regular second order diffusive viscous term replaced by a linear relaxation dependent on the local frictional acceleration $\tan(\delta)g_n$, with δ as friction angle of the material with the base. This assumption has two implications: one, no matter the strength of viscosity, the fluid reaches the same equilibrium, unlike real granular materials; two, g_n causes a reduction of friction near equatorial regions, typical for such systems where equator-ward flowing regolith eventually attains orbital velocity [4].

2.1 Steady-state analysis

Consider a small dune, a local deposit, at a certain non-equatorial location on the sphere with zero rotational frame velocity; see Fig. 1. As time evolves, the dune flows out and material is redistributed on the surface. We assume that at steady state the entire asteroid with its regolith rotates as a rigid body i.e. surface velocities are zero. Under these conditions, we can reduce equation (2) to a balance between the pressure gradient term and the tangential gravitational acceleration. The mass balance (equation (3)) is trivially satisfied as both \mathbf{u} and $\partial h/\partial t$ are zero. Expanding the momentum balance in longitudinal ($\hat{\theta}$) and longitudinal ($\hat{\phi}$) components we get,

$$\left(\frac{h}{R} \frac{\partial g_n}{\partial \theta} + \frac{g_n}{R} \frac{\partial h}{\partial \theta}\right) \hat{\theta} + \left(\frac{g_n}{R \sin \theta} \frac{\partial h}{\partial \phi}\right) \hat{\phi} = g_t \hat{\theta} \quad (4)$$

The ϕ component reduces to the form $\partial h/\partial \phi = 0$, implying that there are no pressure gradients along latitudes at steady-state and the *final height field is axisymmetric*. From the θ component we get a boundary value problem, which we solve using the shooting method, while analytical solutions are also possible. It gives us the steady-state height profile for which the pole to equator gradient is supported by the tangential gravity field. We fix the height distribution by the value of h at the pole, h_{pole} .

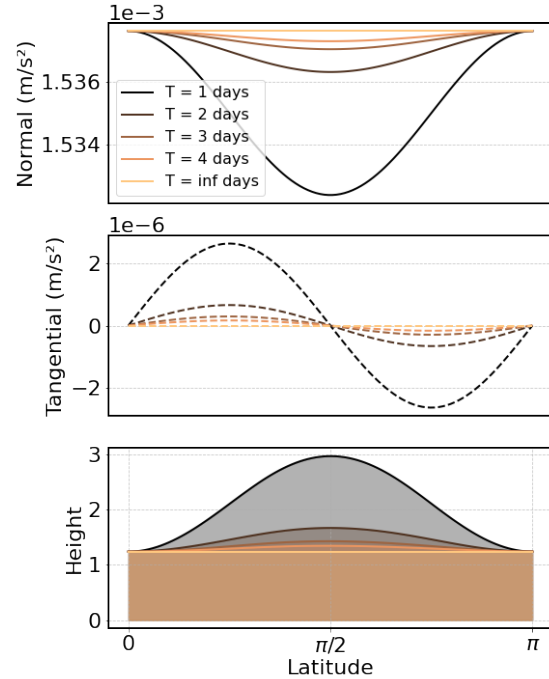


Figure 2. (Top) Variation of the normal component of effective gravitational acceleration (including rotation) across latitudes from the north pole (0 rad) to the south pole (π rad). (Middle) Variation of the tangential component. (Bottom) Analytical solution to steady-state height based on balance obtained in equation (4). The boundary condition is set at the pole to be $h_{pole} = 1.24$ m.

For ease of understanding, we reproduce the effective gravitational acceleration on the surface of a sphere as it varies across latitudes in Fig. 2. The left panel shows the normal component for different rotation periods for a minor planet with radius 1000 m and density 5500 Kg m^{-3} . We see that the equatorial value of the normal gravity reduces with rotation rate, as expected. This contributes not only to the frictional effect as described above but also the pressure gradient term in equation (2). contrary to avalanches on the Earth, where rotation plays little to no role and the gravity field is considered constant.

The second panel shows the tangential component of effective gravity. It is positive in the northern hemisphere and negative in the southern and indicates that a test particle released on the surface always moves towards the equator. Thus, we may expect our initial dune to flow towards the equator under the action of tangential acceleration. This component is contributed to entirely by rotation as gravity is always normal on a sphere.

In panel 3, Fig. 2, we plot the solutions to the linear boundary value problem described in equation (4), with $h_{pole} = 1.24$ m. This value is chosen based on simulation presented later for the benefit of comparison. We see that the steady-state pole to equator gradient of the height field increases with rotation rate. *This implies that a faster-rotating asteroid can support a larger equatorial deposit.* This is commensurate with the equatorial bulge on top-shaped asteroids like Bennu and Ryugu. However,

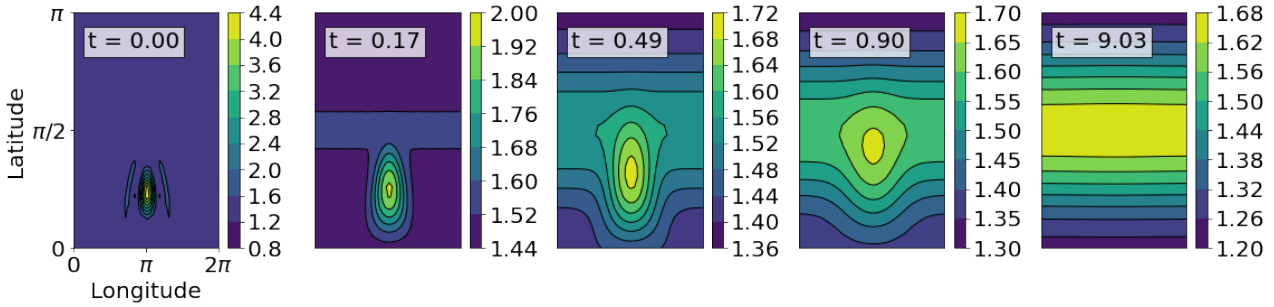


Figure 3. Contours of height for the evolution of a Gaussian dune over a period of 9.03 days. The dune first flows to the equator and then spreads out along $\theta = \pi/2$ leading to the axisymmetric profile predicted in section 2.

the real size of the equatorial deposit should also be limited by the amount of available mobile regolith, which we shall demonstrate later. Additionally, at faster rotation rates, other phenomena like mass shedding can occur further complicating the dynamics [2]. Such cases are left to future work.

Note that the boundary value problem is by definition agnostic to initial conditions. Thus, *no matter the initial location or structure of the dune*, the final state is an axisymmetric height field with a pole to equator gradient. This happens because our system is viscous and will relax to steady-state at infinite time, when equation (4) is valid.

2.2 Numerical method

We use Dedalus3 [6] to solve equations (2) and (3). Dedalus is a pseudo-spectral solver for initial, boundary, or eigen-value problems. It allows the user to enter equations symbolically. We use a sphere basis to discretize our 2-D domain which is then evolved through the RK444 timestepper. The simulation has 32 longitudes and 16 latitudes, which is low but sufficient to capture the central physics phenomena discussed.

3 Results

Similarly as before, we consider a sphere with radius 1000 m and density 5500 Kg m^{-3} . On top of it, a shallow regolith layer of thickness 1.5 m is added. The dune is placed at a latitude of 45 degrees. It has a 2D-gaussian nature with a peak height of 5 m and spread of 9 degrees in latitude and longitude. The rotation period of the sphere is taken as 2 days and the friction angle of regolith, δ is 35 degrees. Note that the frictional term is weighted by \mathbf{u} , which over the course of the simulation is seen to be typically much less than 1. So the effect of friction is smaller than usual. However, this only affects the time to steady-state and not the final solution due to the viscous nature of the resistance as explained in the previous section.

3.1 Dune evolution

Fig. 3 shows the evolution of the initial dune with time. As envisaged from the analysis of the gravity field above,

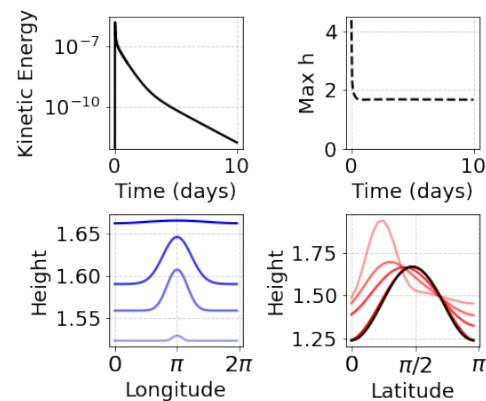


Figure 4. (Top) Evolution of grid averaged kinetic energy and height with time. (Bottom) Time evolution of an equatorial and a polar slice of the height field. For the polar slice, the height distribution is compared with the boundary value solution (black line) and a good quantitative match is found.

the peak of the dune is seen to move towards the equator. Eventually, it slowly spreads out along the equator resulting in the longitude-invariant or axisymmetric steady-state predicted from equation (4). Note that the height field perpetually remains symmetric about the initial longitude of the dune. This happens because the Coriolis term, the creator or asymmetries, is too small at the rotation period of 2 days.

Fig. 4 shows that the kinetic energy in the flow keeps reducing over orders of magnitude due to the \mathbf{u} -dependent resistance term, while the maximum height reaches a steady-state much faster. It also shows the distribution of height along an equatorial slice, showing the gradual build-up and spreading of material, resulting in a constant value at steady-state. In the final panel, the evolution of a polar slice is shown for the longitude at which the dune started initially. The black line is the height profile obtained by solving equation (4), for which the boundary condition (h_{pole}) is informed by the steady-state polar height in Fig. 3, obtained from the simulation. *We find the BVP to match the IVP very closely.* The slight differences is likely due to the truncation of the simulation at 10 days, beyond which the kinetic energy would have further de-

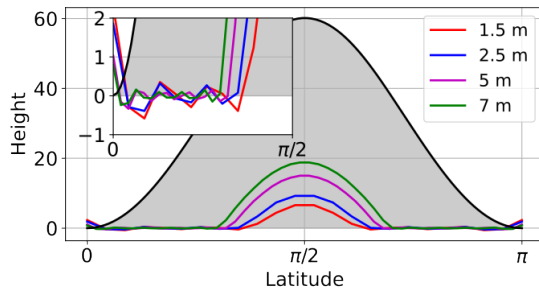


Figure 5. Final height profiles at a higher rotation rate of 4.3 hours. The black line is the solution to the boundary value problem in equation (4) for $h_{pole} = 0$ m. This is compared with simulations starting from a globally uniform regolith layer that eventually accumulates at the equator due to rotational effects. The different lines correspond to different layer thickness. The inset zooms into polar regions, where depletion of material causes the height to go to zero, giving rise to oscillations, a feature of the spectral method used to solve the time-dependent equations.

creased and the final height profile further adjusted to the analytical solution.

It is important to note that the contributions from the Coriolis and advection terms are minimal. This is because rotation is weak and the velocities are small.

3.2 Equatorial bulge and polar singularity

The total amount of available mobile regolith is a crucial factor determining the size of the equatorial bulge. Here this quantity is limited by the initial thickness of the shallow layer and the volume of the dune. Naturally, the greater the thickness of this layer, the greater will be the size of the equatorial bulge. However, we have seen that that the equatorial bulge is also dependent on the rotation period in Sec. 2.

We now consider a faster rotation period of 4.3 hours. The analytical pole to equator height gradient is obtained from equation (4) with the boundary condition $h_{pole} = 0$ m. The deposit is shown by the black line (gray-shaded) region in Fig. 5. We run simulations with the resolution of 32×16 , going up to a height of 7 m for the global regolith thickness. The respective final deposits for each layer thickness is shown in different colors. We find that *the shape of the equatorial bulge is self-similar*. However, for every case, the polar region runs out of material leading to a zero height. Because mass conservation cannot be violated, oscillations build up near polar regions leading to slight negative heights (see inset). This can be resolved using higher resolution and by adding hyperdiffusion that acts strongly on smaller scales [7] but we leave it for later.

4 Conclusions

We have used a spherical shallow water setup to simulate global motion of cohesionless viscous regolith initiated from a *local* gaussian dune placed at a non-equatorial location. From the shallow water equations we derive a bound-

ary value problem at steady-state which can be solved analytically. Having discussed the gravity field of the sphere, we solve the BVP and compare the results with numerical simulations at slow and fast rotation rates.

The steady-state field is longitudinally invariant, thus, under the assumption of viscous flow and over long-time scales, using axisymmetric models may not a bad approximation. The tangential gravity field, contributed to by rotational effects only, causes material migration to the equator resulting in a bulge as seen on many top-shaped asteroids. For our system, the final pole to equator gradient of height is agnostic to the initial conditions. Higher rotation rates can support a stronger pole to equator height gradient, leading to a bigger equatorial bulge, according to analytical solutions. However, numerical simulations show that the size of the bulge is limited by the amount of available mobile regolith.

The principal findings of this study remain robust despite its limitations. For instance, increasing model resolution beyond 32×16 and incorporating hyperdiffusion effectively suppress small-scale oscillations, mitigating the polar singularity, but do not influence the magnitude of the steady-state equatorial bulge, provided the total volume of available regolith is unchanged. While this work adopts a viscous flow model, diverging from granular rheologies with bulk and surface resistance [2, 5], its focus is on analytically tractable edge cases that elucidate first-order dynamics. Such simplified models serve as essential benchmarks for validating more complex simulations. Notably, the final regolith configuration is governed by the total mobile mass and is independent of initial distribution or friction angle, the latter only affecting convergence time. In contrast, granular models require additional mechanisms for dune failure and flow arrest. Rotational effects, addressed analytically in Section 2, predominantly affect the shape of the deposit without altering peak height significantly. Notwithstanding the above caveats, our simplified model helps us understand the overall dynamics of the system at first-order, results from which can serve as comparisons to forthcoming more accurate models.

References

- [1] D.N. Brack, J.W. McMahon, Modeling the coupled dynamics of an asteroid with surface boulder motion, *Icarus* **333**, 96 (2019).
- [2] D. Banik, K. Gaurav, I. Sharma, Proceedings of the Royal Society A **478**, 20210972 (2022).
- [3] D.J. Scheeres, *Icarus* **247**, 1 (2015).
- [4] D. Banik, K. Gaurav, in *52nd Lunar and Planetary Science Conference* (2021), 2548, p. 1122
- [5] K. Gaurav, D. Banik, I. Sharma, P. Dutt, *Journal of Fluid Mechanics* **916**, A40 (2021).
- [6] K.J. Burns, G.M. Vasil, J.S. Oishi, D. Lecoanet, B.P. Brown, *Physical Review Research* **2**, 023068 (2020).
- [7] D. Banik, K. Menou, *Meridional circulation streamlined*, *Geophysical & Astrophysical Fluid Dynamics* **118**, 467 (2024).